# Intracavity dynamics in high-power mode-locked fiber lasers

Brandon G. Bale,[1] Sonia Boscolo,[1] J. Nathan Kutz,[2] and Sergei K. Turitsyn[1]
[1]*Photonics Research Group, School of Engineering and Applied Science, Aston University, Birmingham B4 7ET, United Kingdom*
[2]*Department of Applied Mathematics, University of Washington, Seattle, Washington 98195-2420, USA*
(Received 22 October 2009; published 16 March 2010)

A theoretical model is developed which characterizes the intracavity pulse evolutions in high-power fiber lasers. It is shown that experimentally observed dynamics of the key pulse parameters can be described by a reduced model of ordinary differential equations. Critical in driving the intracavity dynamics is the amplitude and phase modulations generated by the discrete elements in the laser. The theory gives a simple geometrical description of the intracavity dynamics and possible operation modes of the laser cavity. Furthermore, it provides a simple and efficient method for optimizing the performance of complex multiparametric laser systems.

DOI: 10.1103/PhysRevA.81.033828 PACS number(s): 42.55.Wd, 42.81.Dp, 42.65.Tg

## I. INTRODUCTION

Over the past two decades, mode-locked lasers have evolved from the confines of fundamental science to commercial instruments, with a wide variety of applications [1,2]. Currently there is a high level of interest in mode-locked fiber lasers due to the practical advantages they offer such as superior waveguide properties, reduced thermal effects, power scalability, and integrability with other telecom components. Despite much progress in mode-locked fiber lasers, its broader impact has been limited due to restrictions on pulse energies, which is a consequence of the underlying fiber nonlinearities. Indeed, conventional soliton fiber lasers [3] that rely on the balance between anomalous group velocity dispersion (GVD) and self-phase modulation (SPM) only generate pulses with energies up to 0.1 nJ [1,2]. Recently much progress has been made experimentally to achieve high energy, ultrashort pulses from mode-locked fiber lasers. The desire for higher energy pulses suggests consideration of cavities with segments of normal and anomalous GVD or with large and net normal GVD. These include the stretched-pulse laser [4–6], self-similar laser [2,7], and the all-normal dispersion laser [2,8–10]. Indeed, these lasers have increased the pulse energy limits in femtosecond fiber lasers by orders of magnitude. For example, all normal fiber lasers have recently produced pulses with energies approaching the micro-Joule level [10]. A new, interesting direction was found recently in Ref. [11], where by increasing the cavity length of the fiber laser to an impressive 3.8 km, a 3.9-$\mu$J nanosecond (chirped) pulse was demonstrated. In contrast to soliton-like processes [3] where the pulse experiences small changes in the pulse parameters within a single round trip, this new generation of high-power fiber lasers depends strongly on dissipative processes as well as on phase modulations to shape the pulse, often resulting in large intracavity pulse variations per round trip. This requires the development of new, adequate mathematical models for the analysis of such laser systems.

Pulses in mode-locked lasers are referred to generically as dissipative solitons and are usually described within the context of distributed models that captures both the temporal pulse shaping and the propagation in the laser cavity [1]. However, most high-energy fiber lasers rely on large pulse fluctuations per cavity round trip. Specifically, a dispersion map is implemented so pulse solutions may undergo large breathing per cavity round trip [4–6]. Indeed, this concept was exploited in optical communications and fiber transmission [12] where higher energy pulses are possible due to the increased average pulse duration. Furthermore, pulse shaping is dominated by either large phase or amplitude modulations. As a result, modeling the pulsed solution with a distributed partial differential equation (average model) does not fully characterize the intracavity dynamics. Here we provide a semianalytical method to describe the intracavity dynamics in such lasers. In contrast to recent analytical results based upon an averaged Ginzburg-Landau equation [13–15] where the pulse dynamics is averaged over one round trip, we develop a variational method of the fiber propagation equations which includes the essential discrete components that are responsible for large intracavity pulse fluctuations. Such an approximate approach is verified by extensive direct numerical modeling demonstrating the validity of the model. The reduction demonstrates the underlying attracting Poincaré map of the mode-locked solution and highlights how phase profiles, which have been experimentally observed [4–6,8–10], are critical in the mode-locking dynamics. Furthermore, the variational model provides an excellent theoretical framework for multiparametric optimization of the performance of complex laser systems [16]. The article is outlined as follows: In Sec. II, the governing equations for fiber propagation as well as point-wise elements in the laser are introduced which are to be the basis of discussing the variational model. Section III considers the reduced system for both fiber propagation and point-wise elements and highlights the Poincaré mapping for stable mode-locking. Sections IV and V consider the reduced system for a Gaussian ansatz and modified hyperbolic secant ansatz, respectively. Finally, Sec. VI concludes with a short review of the article.

## II. FIBER PROPAGATION EQUATIONS AND DISCRETE ELEMENTS

Pulse propagation in a fiber laser can be modeled with normalized equations that include the dominant physical effects of the system. These effects include GVD, SPM, and attenuation for all fibers, as well as gain saturation and bandwidth limited gain for an active medium such as rare-earth

 

doped fibers [17]. The governing equations are given by

$$iu_z + \tfrac{1}{2}d(z)u_{tt} + \gamma|u|^2u = i(g(z) - \alpha)u + i\nu g(z)u_{tt}, \quad (1)$$

with the saturating gain

$$g(z) = \begin{cases} g_0/[1 + \|u\|^2/e_0] & \text{for active fiber,} \\ 0 & \text{for passive fiber.} \end{cases} \quad (2)$$

Here $u$ represents the electric field envelope normalized by the peak power $P_0$, $\|u\|^2 = \int |u|^2 dt$ is the energy of the pulse, $t$ represents time normalized by $T_0$, and $z$ is the propagation distance normalized by the typical cavity length scale $L$ ($=1$ m). The normalized GVD and SPM coefficients are given by $d(z) = -\beta_2(z)L/T_0^2$ and $\gamma = 2\pi n_2 P_0 L/(\lambda_0 A_{\text{eff}})$, respectively. Here $\beta_2$ is the fiber dispersion coefficient, $n_2$ is the nonlinear refractive index, $\lambda_0$ is the carrier wavelength, and $A_{\text{eff}}$ is the effective fiber area. Equation (1) differs from the well-known nonlinear Schrödinger equation (NLSE) due to the dissipative terms on the right-hand side of the equation, which represents gain saturation, gain dispersion, and linear loss. The dissipative parameters $g_0 = LG$, $e_0 = E_{\text{sat}}/(P_0T_0)$, $\alpha = L\Gamma$, and $\nu = 1/(\Omega_g T_0)^2$ are the normalized small-signal gain coefficient, saturation energy, loss coefficient, and gain dispersion coefficient, respectively. Here $G$ (in 1/meter) is the linear gain from amplification, $\Gamma$ (in 1/meter) is the fiber loss coefficient in the cavity, $E_{\text{sat}}$ (in nanojoules) is the saturation energy of the gain medium, and $\Omega_g$ (in nanometers) is related to the gain bandwidth. The fiber laser also consists of some form of dispersion management (DM), where each segment of fiber can potentially have a different dispersion value. In general, for a fiber laser that consists of $M$ segments of length $L_j$, there will be $M$ dispersion values $d_j$.

In addition to fiber propagation, the pulse experiences action induced by the discrete elements such as a saturable absorber, output coupler, and spectral filter in mode-locked fiber lasers. Indeed, it is necessary to have some form of a saturable absorber (intensity discrimination) to provide self-starting [1]. A variety of different saturable absorber mechanisms have been achieved experimentally and described theoretically in femtosecond mode-locked lasers, including, among others, nonlinear polarization rotation [8,18–20], nonlinear interferometry [21], semiconductor saturable absorber (SESAM) [22–24], and saturable Bragg reflectors [25]. Often, under certain conditions, the action of fast saturable absorbers can be approximated by a simplified, but generic, nonlinear transfer function [1]

$$u_{\text{f}}(t) = \left[1 - \frac{l_0}{1 + |u_{\text{i}}(t)|^2/p_{\text{s}}}\right] u_{\text{i}}(t), \quad (3)$$

where $u_{\text{i}}$ ($u_{\text{f}}$) is the input (output) field, $l_0$ is the unsaturated loss due to the absorber, and $p_{\text{s}} = P_{\text{sat}}/P_0$ is the normalized saturation power. Note that this transfer function effectively promotes high intensities while attenuating lower intensities of the pulse. The discrete action of the output coupler can be approximated by a simple scalar multiplication of the field

$$u_{\text{f}}(t) = \sqrt{\rho} \times u_{\text{i}}(t). \quad (4)$$

In this approximation, we are assuming that the output coupler is only an amplitude modulation and any phase modulations are assumed to be small, so that the laser output field would be given by $\sqrt{1-\rho} \times u_{\text{i}}(z,t)$. Finally, we consider the discrete action of a spectral filter $\hat{A}(\Omega)$ on the pulse. The pulse form is modified in both amplitude and phase and can be written as

$$u_{\text{f}}(t) = \int_{-\infty}^{\infty} \hat{u}_{\text{i}}(\Omega) \times \hat{A}(\Omega)\, e^{-i\Omega t} d\Omega, \quad (5)$$

where $\hat{u}(\Omega)$ denotes the Fourier transform of $u(t)$.

Including all effects of pulse propagation in passive and active fibers as well as the discrete elements of the saturable absorber, output coupler, and spectral filter allows for stable and robust mode-locking in a variety of experimentally realized configurations [1]. Haus proposed that all these effects can be considered in a distributed model of Ginzburg-Landau type that effectively assumes averaging the pulse dynamics over one cavity round trip [1]. However, this distributed model fails when intracavity pulse fluctuations are large. Analysis of modern high-power laser systems in which large modulations within one cavity round trip requires the development of new mathematical approaches. In the following section, we consider the nondistributed model (1)–(5) where parameters characterizing the pulse can change drastically; however, the pulse maintains its form in both the temporal and the spectral domain.

## III. VARIATIONAL REDUCTION AND POINCARÉ MAPPING

Often, pulse propagation through fibers can be characterized by the change of key parameters such as pulse width, power, and chirp, while the pulse keeps its general shape in both the temporal and the spectral domain. Mathematically, this can be treated as a reduction from an infinite dimensional system corresponding to the governing partial differential equation to a finite-dimensional system responsible for the evolution of the key pulse parameters. In other words, the pulse evolves as a particle keeping its identity, rather than as an object built from an infinite set of linear waves that evolve independently. In such a situation one can use a variational method to describe the complete evolution problem with ordinary differential equations that govern the evolution of a finite set of pulse parameters [26]. Variational reductions have been used extensively in nonlinear Schrödinger-type systems to describe the underlying pulse behaviors (see, e.g., [27–30] and references therein). Recent work has focused on variational reductions in the context of mode-locked lasers and general Ginzburg-Landau equations [31–34]. The variational method is traditionally rooted in the Hamiltonian nature of the system (i.e., it is assumed that some conserved energy functional can be constructed). Classical Hamiltonian theory then allows for the construction of the associated Lagrangian via a Legendre transformation. The variational reduction then applies the Euler-Lagrange equations to the free parameters in the ansatz assumption. As exhibited in the following discussion, this leads to ordinary differential equations which determine the evolution of the ansatz parameters.

The right-hand side of (1) represents additional dissipative terms to the NLSE. These terms can be included in the variational method as perturbations to the overall Hamiltonian structure [26]. Assuming a pulse form

$u(z,t) = u_a(p_1(z), p_2(z), \ldots, t)$, where the parameters $p_j(z)$ are $z$ dependent and correspond to the pulse amplitude, duration, chirp, etc., the governing set of ordinary differential equations are given by

$$\frac{\delta}{\delta p_j}\left(\int_{-\infty}^{\infty} L[u_a]dt\right) = 2\mathrm{Re}\left\{\int_{-\infty}^{\infty} i\mathcal{R}[u_a]\frac{\partial u_a^*}{\partial p_j}dt\right\}. \quad (6)$$

The left-hand side of Eq. (6) contains the Hamiltonian contribution, and the right-hand side contains the dissipative perturbations, where

$$L[u] = \frac{i}{2}(u_z u^* - u_z^* u) - \frac{1}{2}d(z)|u_t|^2 + \frac{\gamma}{2}|u|^4, \quad (7)$$

$$\mathcal{R}[u] = [g(z) - \alpha]u + \nu g(z)u_{tt}. \quad (8)$$

The resulting set of ordinary differential equations must be coupled with the discrete action of the saturable absorber, output coupler, and spectral filter. In the phase space of the pulse parameters $p_1, p_2, \ldots p_N$, the flow is determined by the ordinary differential equations (6). When a discrete element is applied, it effectively modifies the pulse parameters $p_j$ in some way. This corresponds to moving the pulse position in the phase plane to another location in the phase plane. In a stable mode-locking configuration, this periodic forcing generates a closed periodic loop, or Poincaré map, in the parameter space $p_1, p_2, \ldots p_N$. Indeed, it is this phase-space representation that highlights the pulse dynamics per cavity round trip. In the following sections, we will obtain explicit ordinary differential equations for particular ansatz functions which represent pulse forms observed in experiments [4–6,8–10]. These reduced set of pulse propagation equations are coupled with the discrete elements in a laser cavity to provide the overall intracavity dynamics.

## IV. REDUCED MODEL FOR GAUSSIAN ANSATZ

Similar to DM systems in communications [12], many high-power mode-locked fiber lasers rely on a strong dispersion map which alternates between normal and anomalous GVD segments. In this case, the pulse can be approximated by a Gaussian-type pulse [12] of the form

$$u_a(t,z) = \sqrt{\eta(z)}\exp\{-[1 - iC(z)][t/\tau(z)]^2 + i\varphi(z)\}. \quad (9)$$

Here $\eta$ is the peak amplitude, $\tau$ is the pulse duration, $C$ is the chirp parameter, and $\varphi$ is the phase parameter. Using (9) in (6) gives the following ordinary differential equations:

$$\eta_z = -2d(z)\frac{C\eta}{\tau^2} + 2(g - \alpha)\eta - 4\nu g\frac{\eta}{\tau^2}, \quad (10)$$

$$\tau_z = 2d(z)\frac{C}{\tau} - 2\nu g\frac{1}{\tau}(C^2 - 1), \quad (11)$$

$$C_z = 2d(z)\frac{1}{\tau^2}(1 + C^2) - \frac{\sqrt{2}}{2}\gamma\eta - 4\nu g\frac{C}{\tau^2}(1 + C^2), \quad (12)$$

where

$$g(z) = \begin{cases} g_0/[1 + \sqrt{\pi/2}\,\eta\tau/e_0] & \text{for active fiber,} \\ 0 & \text{for passive fiber.} \end{cases} \quad (13)$$

Note that the overall phase parameter $\varphi$ is decoupled from the system (10)–(13) (i.e., the system has a phase invariance). The ansatz (9) and the corresponding reduced system (10)–(13) is an extension to that which was successfully used in the context of conservative DM solitons [27,35,36]. The reduced set of ordinary differential equations determines the evolution of the peak amplitude, pulse duration, and chirp parameter in both the active and the passive fiber segments of the laser.

The discrete elements can modify the pulse parameters significantly. To see how the pulse parameters change due to the saturable absorber transfer function (3), we approximate the function

$$\left[1 - \frac{l_0}{1 + \frac{\eta_i}{p_s}e^{-\frac{2t^2}{\tau_i^2}}}\right]\sqrt{\eta_i}\,e^{-(1-iC_i)\frac{t^2}{\tau_i^2}} \sim \sqrt{\eta_f}\,e^{-(1-iC_f)\frac{t^2}{\tau_f^2}}, \quad (14)$$

where the subscript "i" ("f") represents input (output) parameter values. Using a linear least-squares fitting routine, we find that the parameters can be mapped using the functions

$$\eta_f/\eta_i = F_1(l_0, \eta_i/p_s), \quad (15)$$

$$\tau_f/\tau_i = F_2(l_0, \eta_i/p_s), \quad (16)$$

$$C_f/C_i = \tau_i^2/\tau_i^2, \quad (17)$$

where $F_1$ and $F_2$ are shown in Fig. 1. The modulation of $\eta_f$ is independent of $\tau_i$ where it is linear for the pulse duration $\tau_f$. Furthermore, the saturable absorber changes the chirp parameter only due to the change in pulse duration. The simple form of the output coupler (4) translates to a scalar multiplication of the amplitude

$$\eta_f = \rho \times \eta_i. \quad (18)$$

The application of a spectral filter will cause modulation in both the amplitude and the phase parameters. Indeed, spectral filters have been used experimentally to provide additional dispersion compensation, effectively reducing the chirp across a pulse [8,33,37]. To make analytical progress, we assume a Gaussian profile for the spectral filter $\hat{A}(\Omega) = \exp[-\Omega^2/(4\Omega_f^2)]$ so that we can calculate the integral (5). After transforming (9), multiplying by $\hat{A}(\Omega)$ and integrating, we obtain a Gaussian pulse with modified parameters

$$\eta_f = \left(\frac{\tau_i}{\sqrt[4]{a^2 + b^2}}\right)\eta_i, \quad (19)$$

$$\tau_f = \sqrt{\frac{a^2 + b^2}{a + b^2}}, \quad (20)$$

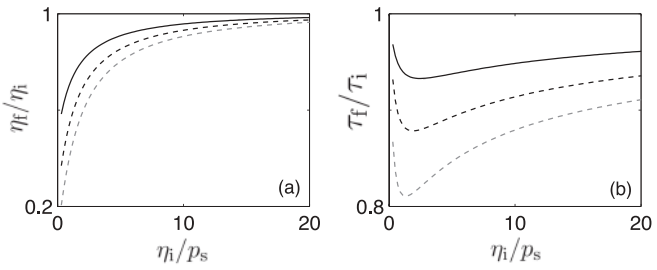


FIG. 1. Peak-power (a) and pulse duration (b) modulations from the discrete action of the saturable absorber (3) on a Gaussian pulse for the parameter values $l_0 = 0.3$ (solid), 0.5 (dashed black), and 0.7 (dashed gray).

$$C_{\mathrm{f}} = \left(\frac{\tau_{\mathrm{i}}^4}{a^2 + b^2}\right) C_{\mathrm{i}}, \tag{21}$$

where $a = \tau_{\mathrm{i}}^2 + 1/\Omega_f^2$ and $b = \tau_{\mathrm{i}}^2 C_{\mathrm{i}}/\Omega_f$. Note that as $\Omega_f \to \infty$, $a \to \tau_{\mathrm{i}}^2$ and $b \to 0$ resulting in no modification of the pulse parameters. For a finite filter bandwidth, the spectral filter reduces the chirp parameter by a factor that is inversely proportional to the ratio of chirp parameter to filter bandwidth. Thus, the larger the chirp value, the more it will get reduced. Furthermore, the spectral filter induces a significant amplitude modulation in both peak power and pulse duration.

With the system of fiber propagation equations (10)–(13) and discrete operations (15)–(21), we can solve the reduced set of equations and compare them with numerical simulations of the full equations for a particular laser system. Figure 2 shows an example of the resulting pulse evolution from numerical simulation of (1)–(2) consisting of an active fiber segment of length $L_1 = 1$ with normal dispersion $d_1 = -0.9$ followed by a passive segment of length $L_2 = 1$ with anomalous dispersion $d_2 = 1$. Thus, the net-dispersion $\bar{d} = 0.05$ is in the anomalous dispersion regime. A saturable absorber and output coupler follow the passive segment. The initial condition is white noise; thus, the pulse evolution is, in a global sense, the final attracting state. This fiber laser setup is similar to that where stretched pulse operation was achieved in Ref. [4]. Note that the discrete elements cause the pulse to undergo large changes in its pulse parameters; however, the pulse shape

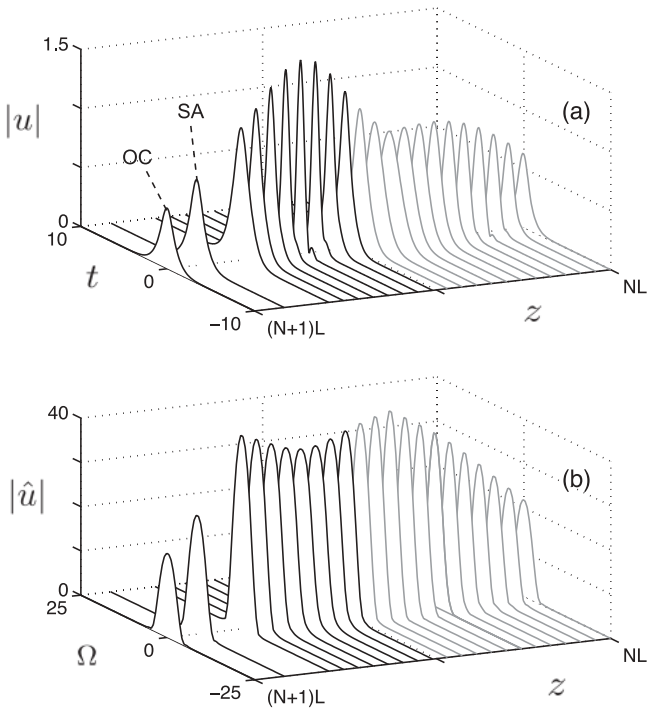


FIG. 2. Temporal (a) and spectral (b) solutions from numerical simulation of (1) with gain (2) in the net-anomalous dispersion regime. Dispersion map parameters are $d_1 = 1$, $L_1 = 1$, and $d_2 = -0.9$, $L_2 = 1$. Dissipative parameters are $g_0 = 2$, $e_0 = 1$, $\nu = 0.05$, $\alpha = 0.1$, $l_0 = 0.5$, $p_s = 3$, and $\rho = 0.5$. Note that the saturable absorber (SA) and output coupler (OC) are applied at the end of the map resulting in last two pulses. Gray shade corresponds to the gain segment.

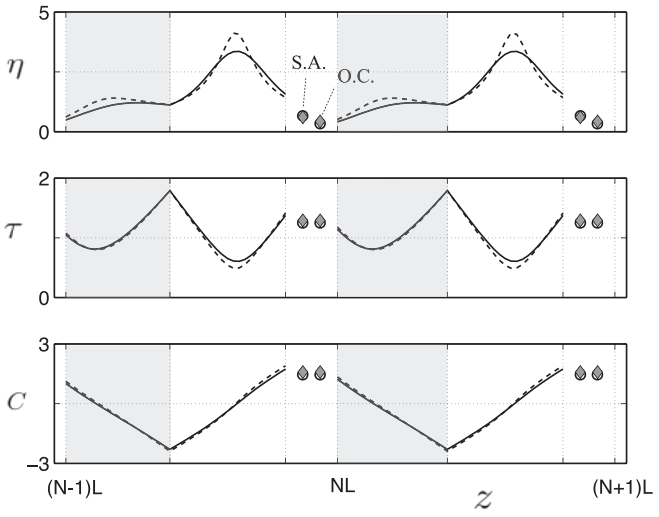


FIG. 3. Evolution of pulse parameters over two map periods from full simulations (solid) and the reduced system (dashed) for the laser setup in Fig. 2. The results from application of the saturable absorber (SA) and output coupler (OC) are shown for both the full (circle) and reduced (gray diamonds) models. Shaded regions correspond to the gain segment.

remains of Gaussian form. Figure 3 shows the comparison of the pulse parameters from full numerical simulation and from solving the reduced system (10)–(13) and discrete operations (15)–(18). The initial condition for the reduced model was $[\eta_0, \tau_0, C_0] = [0.1, 1, 0.1]$. The final periodic state is obtained from a wide variety of initial conditions and is indeed the attracting state. Although the reduced model is constrained by the ansatz (9), it is remarkable how accurately it models the full equation dynamics. It is clear from Fig. 3 that the pulse compress twice per cavity round trip, reach a minimum duration in the middle of each segment, and acquire both signs of chirp. Furthermore, the saturable absorber and output coupler reduce the peak power of the pulse; however, they only slightly perturb the pulse duration and chirp parameter once the pulse has settled into its stable periodic state.

In general, characterizing the laser requires an investigation of a very large parameter space. Typically many numerical simulations of the full governing equations are needed to completely understand the different modes of operation. The accuracy of the reduced model in characterizing the pulse evolution in the laser allows for one to do these simulations at a reduced computational price. Specifically, the laser can be analyzed by numerically solving the $(3 \times 3)$ system (10)–(13) followed by scalar multiplications for the discrete elements per round trip. In contrast, simulations of the full equations (1) involve solving an $(N \times N)$ system ($N$ large) after discretization. Figure 4 shows the phase plane of the intracavity dynamics in the experimentally relevant phase plane of pulse energy $E$, duration $\tau$, and chirp parameter $C$. The periodic application of the saturable absorber and output coupler (once per round trip) actively controls the parameters of the mode-locked pulse. Here, after application of the saturable absorber, the phase point is moved to the black diamond. The output coupler moves the phase point to the gray circle, where then the solution evolves along the flow line shown. The geometrical picture presented here gives a way to

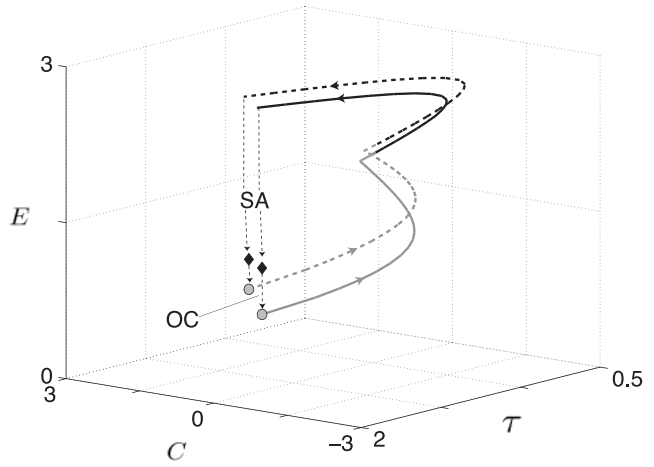


FIG. 4. Poincaré map of stable mode-locking operation of Fig. 2. The jump condition associated with the saturable absorber results in the flow moving to the black diamond, while that associated with the output coupler moves the phase point to the gray circle. The solid lines correspond to the full model (1–4), and the dashed lines correspond to the reduced model (10)–(13) illustrating good agreement. Gray segments correspond to the gain fiber segment.

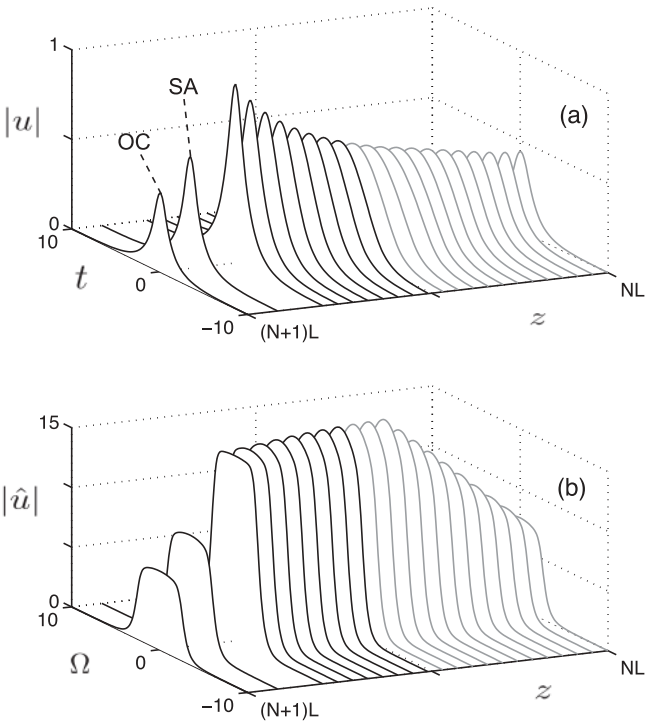


FIG. 5. Temporal (a) and spectral (b) solutions from numerical simulation of (1) with gain (2) in the net-normal dispersion regime. The laser setup is the same as in Fig. 2 but with $d_2 = -1.2$. Gray shade corresponds to the gain segment.

rapidly predict the intramap pulse evolutions and to optimize the laser cavity for optimal performance.

There are many laser systems where a Gaussian pulse form in both the temporal and the spectral domains is violated. Indeed, the reduced model can be used for a wide variety of pulse ansatz. However, it is interesting that the Gaussian ansatz used to obtain the reduced model (10)–(13) and the discrete operations (15)–(18) does remarkably well in characterizing pulse dynamics even when the pulse is not of Gaussian form. For example, Fig. 5 shows the temporal and spectral evolution with the same laser configuration as in Fig. 2, but with a dispersion parameter $d_2 = -1.2$ giving a net-dispersion $\bar{d} = -0.1$. Indeed, at some points in the map the spectrum has a flat-top profile with steep sides which is characteristic in normal-dispersion mode-locking [1]. Figure 6 shows the pulse evolutions over two map periods from both the full Eqs. (1)–(4) and the reduced model (10)–(13) with discrete actions (15)–(18). Note that in contrast to the net-anomalous dispersion laser, here the pulse compresses once per cavity round trip and is positively chirped throughout the cavity. Because the Gaussian trial function parameters can be related to the pulse integral characteristics (see, e.g., [12,38]), in many cases the overall reduced system does not depend heavily on the actual pulse form. However, there are laser setups that demand pulse forms that have more complicated spectral profiles [2,8,9]. In the following section, we obtain a reduced set of ordinary differential equations that govern the pulse parameters of an ansatz that is capable of describing such features.

## V. REDUCED MODEL FOR MODIFIED CHIRPED-SECH ANSATZ

Recently there has been much interest and progress in generating high-power pulses in a fiber laser that consists of all-normal dispersion elements. To control the dispersive spectral broadening, a spectral filter is placed within the laser cavity. These lasers can have rounded-top or flat-top spectral profiles, as well as spectral profiles with peaks at its edges [8–10]. To fully capture the varying spectral profiles which have been observed in these all-normal fiber lasers, we

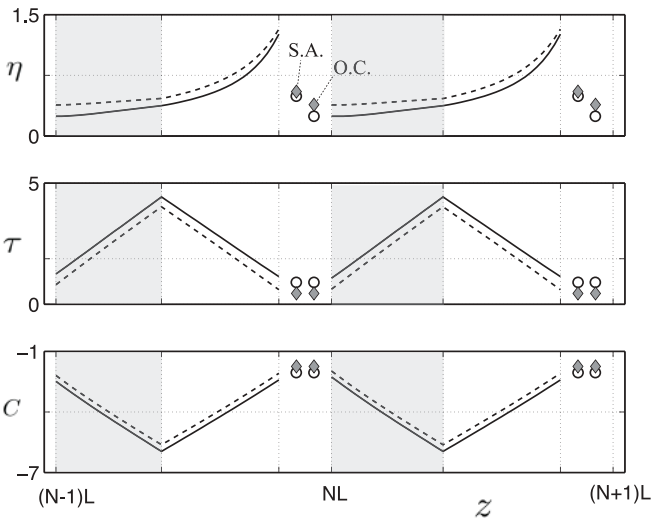


FIG. 6. Evolution of pulse parameters over two map periods from full simulations (solid) and the reduced system (dashed) for the laser setup in Fig. 5. The results from application of the saturable absorber (SA) and output coupler (OC) are shown for both the full (circle) and the reduced (gray diamonds) models. Shaded regions correspond to the gain segment.

assume a modified chirped hyperbolic secant ansatz of the form [9]

$$u_a(t,z) = \sqrt{\frac{\eta(z)}{B(z)+\cosh\left(\frac{t}{\tau(z)}\right)}}\, e^{-i\frac{C(z)}{2}\ln[B(z)+\cosh(t/\tau(z))]}. \quad (22)$$

The specific form of the phase profile is essential to capture the different spectral profiles observed experimentally [8–10]. Furthermore, ansatz (22) is general and can capture many pulse shapes in both the temporal and the spectral domains. Using (22) in (6) gives the following system of ordinary differential equations:

$$M\vec{f} = \vec{q}, \quad (23)$$

where

$$M = \begin{bmatrix} 0 & CF & \tau G & -\tau CF' \\ -CF & 0 & \eta(G-F) & -2\eta CF' \\ -\tau G & \eta(F-G) & 0 & -\eta\tau(F'+G') \\ \tau CF' & 2\eta CF' & \eta\tau(F'+G') & 0 \end{bmatrix}, \quad (24)$$

$\vec{f} = [\eta, \tau, C, B]_z$, and the components in the vector $\vec{q}$ include the terms from dispersion, self-phase modulation, and the gain and loss perturbations. Neglecting gain dispersion ($\nu = 0$), we have

$$q_1 = \frac{d(z)}{4}\frac{(1+C^2)}{\tau}Q + 2\gamma\eta\tau F', \quad (25)$$

$$q_2 = \frac{-d(z)}{4}\frac{\eta(1+C^2)}{\tau^2}Q + \gamma\eta^2 F' + 2(g-\alpha)\eta CF, \quad (26)$$

$$q_3 = \frac{d(z)}{2}\frac{\eta C}{\tau}Q - 2(g-\alpha)\eta\tau G, \quad (27)$$

$$q_4 = \frac{d(z)}{4}\frac{\eta(1+C^2)}{\tau}Q' + \gamma\eta^2\tau F'' + 2(g-\alpha)\eta\tau CF', \quad (28)$$

where

$$g(z) = \begin{cases} g_0/\left[1+\eta\tau F/e_0\right] & \text{for active fiber,} \\ 0 & \text{for passive fiber.} \end{cases} \quad (29)$$

All primes denote differentiation with respect to the parameter $B$, and the parameters $F$, $G$, and $Q$ are $B$-dependent integrals given by

$$F = \int \frac{dt}{\Theta}, \quad G = \int \frac{\ln\Theta dt}{\Theta}, \quad Q = \int \frac{\sinh^2 t\, dt}{\Theta^3},$$

with $\Theta = B + \cosh t$ and all integrations ranging from $t \in [-\infty, \infty]$.

For the ansatz (22), obtaining analytic expressions for how the pulse parameters change due to discrete operations is difficult. However, a simple least-squares fit between the modified pulse and ansatz (22) in both the temporal and the spectral domains allows for the modified parameters to be obtained. Indeed, ansatz (22) has more fitting parameters than the Gaussian ansatz (9), thus allowing for a wide variety of pulse forms.

Figure 7 shows the final steady state of a laser consisting of $L_1 = 3$ of passive fiber, followed by a gain segment with $L_2 = 0.6$, which is then followed by a passive fiber of length $L_3 = 1$. All segments of the fiber have normal dispersion value

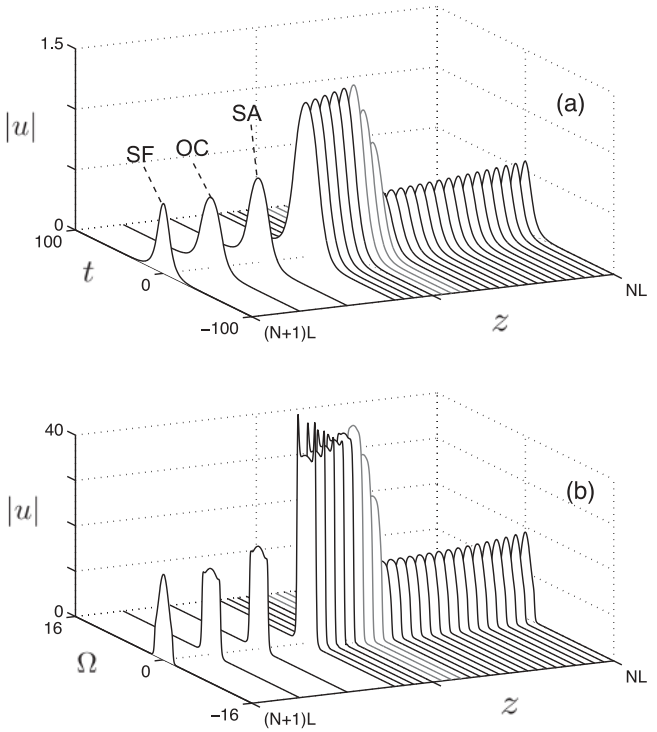


FIG. 7. Temporal (a) and spectral (b) solutions from numerical simulation of (1) with gain (2) for an all-normal dispersion laser. Dispersion map parameters are $d_1 = -1, L_1 = 3, d_2 = -1, L_2 = 0.6$, and $d_3 = -1, L_3 = 1$, and $\gamma = 2$. Dissipative parameters are $g_0 = 30$, $e_0 = 1, \nu = 0, \alpha = 0, l_0 = 0.5, p_s = 3, \rho = 0.7$, and $\Omega_f = 0.8$. Note that the saturable absorber (SA), output coupler (OC), and spectral filter (SF) are applied in series resulting in the last three pulses in the map. Gray shade corresponds to the gain segment.

$d = -1$. These fiber segments are followed by a saturable absorber, output coupler, and spectral filter, respectively. The spectral filter is of Gaussain form as in the previous section. This laser is similar in design to that in Ref. [8]. Note that the temporal and spectral profiles clearly show various states of the ansatz (22) with rounded-top, flat-top, and fringed spectral profiles. Figure 8 shows the comparison of the physically relevant quantities energy [$E = \eta\tau F(B)$], peak power [$Q = \eta/(1+B)$], pulse duration ($\tau$), and chirp parameter ($C$) over two map periods from the full governing Eqs. (1)–(2) with that obtained from the reduced model (23). The modified parameters as a result of the discrete elements were obtained by a linear least-squares fit of the resulting pulse with ansatz (22). Figures 9 and 10 show the temporal and spectral profiles of the pulse solution from the full governing Eqs. (1)–(2) as well as the ansatz (22) with parameter values given by the solutions to the reduced Eq. (23) at four distinct locations in the cavity. It is clear that the reduced model does an excellent job in describing the overall structure of the mode-locked solution throughout the laser cavity. Furthermore, the reduced model captures the main features observed experimentally in all-normal dispersion lasers such as a large, increasing pulse duration and chirp parameter per cavity round trip [8]. The discrete elements reduce these pulse parameters. Indeed, it is interesting that for the ansatz (22) the saturable absorber and output coupler

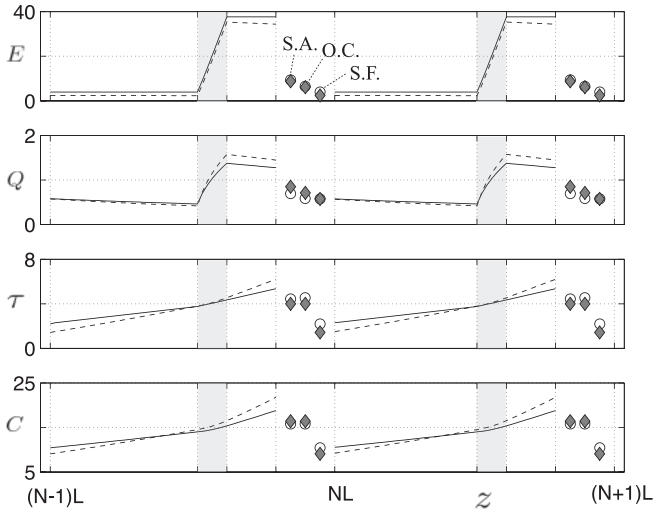


FIG. 8. Evolution of pulse parameters over two map periods from full simulations (solid) and the reduced system (dashed) for the laser setup in Fig. 7. The results from application of the saturable absorber (SA), output coupler (OC), and spectral filter (SF) are shown for both the full (circle) and reduced (gray diamonds) models. Shaded regions correspond to the gain segment.

induce large phase modulations due to the phase parameter $B$ in the amplitude. Again, the reduced system captures the overall dynamics at a fraction of the computational cost: solving a $(4 \times 4)$ system with six (three temporal, three spectral) least-squares fits per round trip. Thus, the reduced system can be used to explore various modes of laser operation quickly. As an example, Fig. 11 shows the output pulse energy over a range of spectral filter bandwidth values $\Omega_f$. Two laser configurations are considered, where all parameters are the same as in Fig. 7, but the order of the saturable absorber and the output coupler are switched. All output energies are

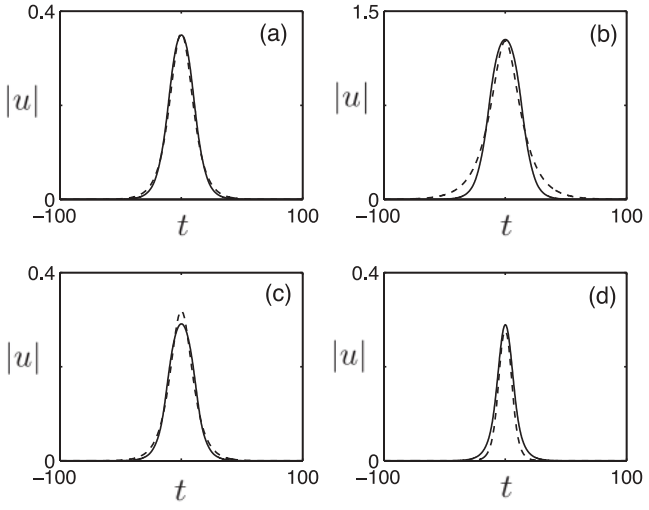


FIG. 9. Temporal profiles of the pulse solution from the full governing Eqs. (1)–(2) (solid) as well as the ansatz (22) with parameter values given by the solutions to the reduced Eq. (23) (dashed) at four distinct locations in the cavity. (a) At the beginning of the gain segment; (b) at the end of the gain segment; (c) after the output coupler; and (d) after spectral filtering.

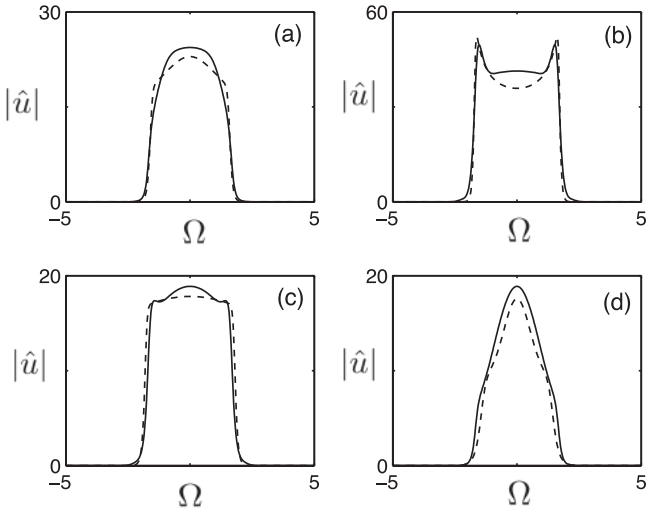


FIG. 10. Spectral profiles of the pulse solution from the full governing Eqs. (1)–(2) (solid) as well as the ansatz (22) with parameter values given by the solutions to the reduced Eq. (23) (dashed) at the same four distinct locations in the cavity as in Fig. 9.

normalized by the output pulse energy of the laser system considered in Fig. 7. It is clear that stable mode-locking exists over a broad range of filter bandwidths and the output energy does not depend heavily on the filter bandwidth. Furthermore, by placing the output coupler before the saturable absorber, the output pulse energy can be significantly increased by a factor of three or four. The output energies obtained from direct numerical simulations of Eqs. (1)–(2) confirm the validity of the reduced model. Although here we have only considered

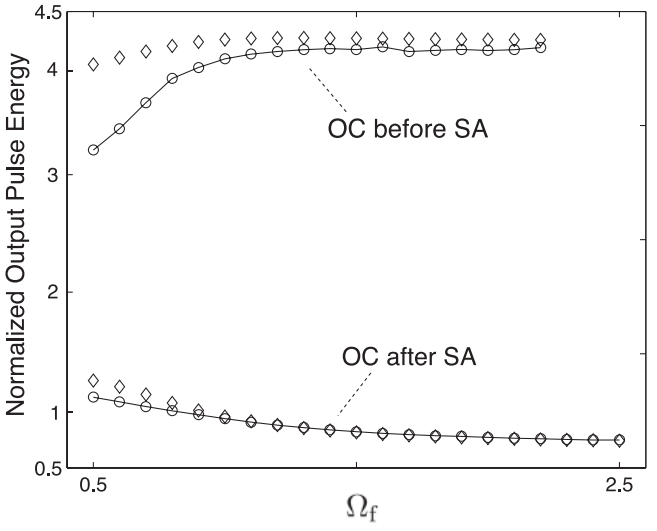


FIG. 11. Output pulse energies as a function of spectral filter bandwidth values $\Omega_f$ for two laser configurations from both the full governing Eqs. (1)–(2) (diamonds) and the reduced model (23). All parameters are the same as in Fig. 7, but the order of the saturable absorber and the output coupler are switched. All output energies are normalized by the output pulse energy of the laser system considered in Fig. 7. The output pulse energies are significantly increased in the configuration where the output coupler precedes the saturable absorber.

two variations in the laser cavity, the reduced model can be used efficiently to explore the multiparametric system and optimize the performance of the laser. Future directions will be to use the reduced system to obtain optimal modes of operation experimentally.

## VI. CONCLUSION AND APPLICATION OUTLOOK

In conclusion, we have considered the large pulse fluctuations in high-energy fiber lasers. We have shown that the intracavity dynamics can be modeled by a reduced set of ordinary differential equations governing the evolution of the pulse parameters. The discrete elements are included as a periodic forcing and generate a closed Poincaré loop for the evolution. The variational method used here provides a geometrical interpretation which is in good agreement with the intracavity temporal and spectral profiles observed in numerical and experimental results. Indeed, the accuracy of the reduced model allows for a large multiparameter analysis of the laser performance to be made at a fraction of the computational cost when compared with full numerical simulations. Furthermore, the location of the output coupler, saturable absorber, and spectral filter can be readily and easily moved within the cavity to explore various modes of operation while full simulations would make this impractical. This simple geometric approach allows for the engineering of cavities to achieve peak performance in both peak power and pulse energies. This mathematical formalism could potentially have a broad impact in the design and development of fiber lasers.

## ACKNOWLEDGMENTS

The authors would like to acknowledge Keith Blow, Frank Wise, and Sergey Kobtsev for fruitful discussions. B. G. Bale acknowledges the support by the Royal Society and the Engineering and Physical Sciences Research Council (Grant No. EP/FO2956X/1). J. N. Kutz also acknowledges support from the National Science Foundation (NSF) (DMS-0604700) and the US Air Force Office of Scientific Research (AFOSR) (FA9550-09-0174).

[1] H. A. Haus, IEEE J. Sel. Top. Quantum **6**, 1173 (2000).
[2] F. W. Wise, A. Chong, and W. H. Renninger, Laser Photon. Rev. **2**, 58 (2008).
[3] L. F. Mollenauer and J. P. Gordon, *Solitons in Optical Fibers: Fundamentals and Applications* (Academic Press, New York, 2006).
[4] K. Tamura, E. P. Ippen, H. A. Haus, and L. E. Nelson, Opt. Lett. **18**, 1080 (1993).
[5] J. R. Buckley, F. W. Wise, F. O. Ilday, and T. Sosnowski, Opt. Lett. **30**, 1888 (2005).
[6] F. O. Ilday, F. W. Wise, and T. Sosnowski, Opt. Lett. **27**, 1531 (2002).
[7] F. O. Ilday, J. R. Buckley, W. G. Clark, and F. W. Wise, Phys. Rev. Lett. **92**, 213902 (2004).
[8] A. Chong, W. H. Renninger, and F. W. Wise, J. Opt. Soc. Am. B **25**, 140 (2008).
[9] W. H. Renninger, A. Chong, and F. W. Wise, Phys. Rev. A **77**, 023814 (2008).
[10] B. Ortac, M. Baumgartl, J. Limpert, and A. Tunnermann, Opt. Lett. **34**, 1585 (2009).
[11] S. Kobtsev, S. Kukarin, and Y. Fedotov, Opt. Express **16**, 21936 (2008).
[12] S. K. Turitsyn, E. G. Shapiro, S. B. Medvedev, M. P. Fedoruk, and V. K. Mezentsev, Comptes Rendus Physique, Académie des sciences/Éditions scientifiques et médicales **4**, 145 (2003).
[13] V. L. Kalashnikov and A. Apolonski, Phys. Rev. A **79**, 043829 (2009).
[14] E. Podivilov and V. L. Kalashnikov, JETP Lett. **82**, 467 (2005).
[15] J. M. Soto-Crespo, M. Grapinet, P. Grelu, and N. N. Akhmediev, Phys. Rev. E **70**, 066612 (2004).
[16] B. G. Bale, J. N. Kutz, A. Chong, W. H. Renninger, and F. W. Wise, Opt. Lett. **33**, 941 (2008).
[17] G. P. Agrawal, *Nonlinear Fiber Optics* (Academic Press, New York, 2007).
[18] V. J. Matsas, T. P. Newson, D. J. Richardson, and D. N. Payne, Electron. Lett. **28**, 1391 (1992).
[19] M. E. Fermann, M. J. Andrejco, Y. Silverberg, and M. L. Stock, Opt. Lett. **18**, 894 (1993).
[20] A. Komarov, H. Leblond, and F. Sanchez, Phys. Rev. E **72**, 025604(R) (2005).
[21] I. N. Duling, Electron. Lett. **27**, 544 (1991).
[22] I. D. Jung, F. X. Kartner, N. Matuschek, D. H. Sutter, F. Morier-Genoud, G. Zhang, U. Keller, V. Scheuer, M. Tilsch, and T. Tschudi, Opt. Lett. **22**, 1009 (2008).
[23] R. Herda and O. Okhotnikov, IEEE J. Quantum Electron. **40**, 893 (2004).
[24] O. Shtyrina, M. Fedoruk, S. Turitsyn, R. Herda, and O. Okhotnikov, J. Opt. Soc. Am. B **26**, 346 (2009).
[25] B. Collings, S. Tsuda, S. Cundiff, J. N. Kutz, M. Koch, W. Knox, and K. Bergman, IEEE J. Select. Top. Quantum Electron. **3**, 1065 (1997).
[26] A. Bondeson, M. Lisak, and D. Anderson, Phys. Scr. **20**, 479 (1979).
[27] I. Gabitov and S. K. Turitsyn, JETP Lett. **63**, 861 (1996).
[28] J. N. Kutz, P. Holmes, S. G. E. Jr., and J. P. Gordon, J. Opt. Soc. Am. B **15**, 87 (1998).
[29] B. A. Malomed, Prog. Opt. **43**, 69 (2002).
[30] A. Mikhailov, in *Optical Solitons: Theoretical Challenges and Industrial Perspective*, edited by V. Zakharov and S. Wabnitz (Springer, New York, 1999), p. 63.
[31] N. Usechak and G. P. Agrawal, Opt. Express **13**, 2075 (2005).
[32] B. G. Bale and J. N. Kutz, J. Opt. Soc. Am. B **25**, 1193 (2008).
[33] B. G. Bale, S. Boscolo, and S. K. Turitsyn, Opt. Lett. **34**, 3286 (2009).
[34] W. Chang, A. Ankiewicz, J. M. Soto-Crespo, and N. Akhmediev, J. Opt. Soc. Am. B **25**, 1972 (2008).

[35] S. K. Turitsyn, I. Gabitov, E. W. Laedke, V. K. Mezentsev, S. L. Musher, E. G. Shapiro, T. Schafer, and K. H. Spatschek, Opt. Commun. **151**, 117 (1998).
[36] J. N. Kutz and S. G. Egangelides, Opt. Lett. **23**, 685 (1998).
[37] S. K. Turitsyn and E. G. Shapiro, J. Opt. Soc. Am. B **16**, 1321 (1999).
[38] S. K. Turitsyn, T. Schaefer, and V. K. Mezentsev, Phys. Rev. E **58**, R5264 (1998).